GEOPHYSICS, VOL. 59, NO. 12 (DECEMBER 1994); P. 1911-1919, 9 FIGS.

The wave equation in generalized coordinates

Jose M. Carcione*

ABSTRACT

This work introduces a spectral collocation scheme for the viscoelastic wave equation transformed from Cartesian to generalized coordinates. Both the spatial derivatives of field variables and the metrics of the transformation are calculated by the Chebychev pseudospectral method. The technique requires a special treatment of the boundary conditions, which is based on 1-D characteristics normal to the boundaries. The numerical solution of Lamb's problem requires two 1-D stretching transformations for each Cartesian direction. The results show excellent agreement between the elastic numerical and analytical solutions, demonstrating the effectiveness of the differential operator and boundary treatment. Another example, requiring 1-D transformations, tests the propagation of a Rayleigh wave around a corner of the numerical mesh. Two-dimensional transformations adapt the grid to topographic features: a syncline, and an anticlinal structure formed with fine layers.

INTRODUCTION

Many problems need coordinate transformations so as to conform to boundaries of a physical region. For instance, in geophysical problems it is important to properly simulate the different types of waves generated at interfaces, for instance, Rayleigh and Love waves at the surface of the earth and Stoneley waves propagating between geological formations. In general, these interfaces have irregular shapes, like the earth's topography or the configuration formed by an oil well, the formations, and the surface. Moreover, for anelastic waves, accuracy is very important. In this sense, spectral differential operators are free of numerical dispersion up to the Nyquist wavenumber.

The generalized coordinates in spectral methods were first introduced by Orszag (1980) to solve fluid dynamic problems. Fornberg (1988), and recently Nielsen et al. (1992), used coordinate transformations to accurately represent interfaces, in this way avoiding the unphysical noise produced by the discretization. Their method uses the Fourier method in two dimensions to compute the spatial derivatives, and therefore is restricted only to periodic boundary conditions. Geophysical applications based on the Fourier/Chebychev differential operator include the works of Kessler and Kosloff (1990), who solved the acoustic wave equation in cylindrical coordinates and Tessmer et al. (1992a, b), who modeled elastic seismic waves in the presence of surface topography. Kosloff et al. (1990) and Carcione (1992a) simulated elastic and anelastic Rayleigh waves, respectively, in a planar surface by using the same operator. However, as before, the modeling algorithm is restricted to periodic boundary conditions in one of the directions.

Raggio (1986) first introduced a 2-D Chebychev differential operator to solve the acoustic wave equation. The disadvantage of his approach is that the collocation points are restricted to the Gauss-Lobatto points.1 This restriction not only produces a lack of flexibility in defining the material interfaces but also greatly restricts the time step required for stabilizing the time integration technique. In this work, I extend Raggio's modeling scheme from the acoustic case to viscoelastic rheology and use a mapping transformation that circumvents the severe stability condition and distributes grid points in arbitrary locations. This spatial grid adaptation concept was already applied by Augenbaum (1989, 1990) to the 1-D wave equations solved with the Fourier method. Applications of the algorithm to the Navier-Stokes equation and to ultrasonic problems in elastic media can be found in Wang et al. (1991) and Carcione and Wang (1993), respectively .

A 2-D generalized curvilinear mapping transforms the physical domain into a computational domain where the spatial derivatives are calculated by the 2-D Chebychev

'They correspond to the Chebychev-Gauss Lobatto quadrature points and are related to the roots of a linear combination of Chebychev polynomials.

Presented at the 63rd Annual International Meeting, Society of Exploration Geophysicists. Manuscript received by the Editor September 15, 1993; revised manuscript received May 9, 1994.
* Osservatorio Geofisico Sperimentale, P.O. Box 2011 Opicina, 34016 Trieste, Italy.

operator. In this way, arbitrary shaped bodies bounded by continuous curves and continuous interfaces can be treated. However, the conventional Chebychev operator requires very small time steps depending on the super-fine grid near the boundaries. Then, for each coordinate, a 1-D stretching function is applied that circumvents the severe stability condition. The nonperiodic properties of the Chebychev operator allow the implementation of general boundary conditions such as free surface, nonreflecting, or open boundaries, etc. Since a direct application of the boundary conditions produces numerical instabilities, a boundary treatment based on the decomposition of the wave equation into incoming and outgoing characteristics (Carcione, 1992b) is implemented. The algorithm uses an explicit fourth-order Runge-Kutta integration scheme for time marching (Carcione 1992a).

THE WAVE EQUATION

The wave equation is based on the equation of momentum conservation combined with the constitutive relations for 2-D isotropic and viscoelastic media (Carcione, 1992a). Here, for simplicity, one dissipation mechanism is considered for each body wave. The boundary treatment requires a velocity-stress formulation that takes the following matrix form:

$$\frac{\partial \mathbf{v}}{\partial t} = \underline{\mathbf{A}}\,\frac{\partial \mathbf{v}}{\partial x} + \underline{\mathbf{B}}\,\frac{\partial \mathbf{v}}{\partial y} + \mathbf{s}, \tag{1}$$

where

$$\mathbf{v} = [v_x,\ v_y,\ \sigma_{xx},\ \sigma_{yy},\ \sigma_{xy},\ \varepsilon_1,\ \varepsilon_2,\ \varepsilon_3]^T \tag{2a}$$

is the vector of unknown variables,

$$\mathbf{s} = \left[f_x,\ f_y,\ (\lambda+\mu)\varepsilon_1 + \mu\varepsilon_2,\ (\lambda+\mu)\varepsilon_1 + \mu\varepsilon_2,\ \mu\varepsilon_3,\ \frac{-\varepsilon_1}{\tau_\sigma^{(1)}},\ \frac{-\varepsilon_2}{\tau_\sigma^{(2)}},\ \frac{-\varepsilon_3}{\tau_\sigma^{(2)}},\right]^T, \tag{2b}$$

with

$$\underline{\mathbf{A}} = \begin{bmatrix} 0 & 0 & \rho^{-1} & 0 & 0 & 0 & 0 & 0 \\ 0 & 0 & 0 & 0 & \rho^{-1} & 0 & 0 & 0 \\ \hat{E} & 0 & 0 & 0 & 0 & 0 & 0 & 0 \\ \hat{\lambda} & 0 & 0 & 0 & 0 & 0 & 0 & 0 \\ 0 & \hat{\mu} & 0 & 0 & 0 & 0 & 0 & 0 \\ \phi_1 & 0 & 0 & 0 & 0 & 0 & 0 & 0 \\ \phi_2 & 0 & 0 & 0 & 0 & 0 & 0 & 0 \\ 0 & \phi_2 & 0 & 0 & 0 & 0 & 0 & 0 \end{bmatrix}, \tag{3a}$$

and

$$\underline{\mathbf{B}} = \begin{bmatrix} 0 & 0 & 0 & 0 & \rho^{-1} & 0 & 0 & 0 \\ 0 & 0 & 0 & \rho^{-1} & 0 & 0 & 0 & 0 \\ 0 & \hat{\lambda} & 0 & 0 & 0 & 0 & 0 & 0 \\ 0 & \hat{E} & 0 & 0 & 0 & 0 & 0 & 0 \\ \hat{\mu} & 0 & 0 & 0 & 0 & 0 & 0 & 0 \\ 0 & \phi_1 & 0 & 0 & 0 & 0 & 0 & 0 \\ 0 & -\phi_2 & 0 & 0 & 0 & 0 & 0 & 0 \\ \phi_2 & 0 & 0 & 0 & 0 & 0 & 0 & 0 \end{bmatrix}, \tag{3b}$$

where $\hat{E} = \hat{\lambda} + 2\hat{\mu}$. In the preceding equations, $\mathbf{x} = (x, y)$ are the Cartesian coordinates, $v_x(\mathbf{x}, t)$ and v_y (x, t) are the particle velocities, $\sigma_{xx}(\mathbf{x}, t)$, σ_{yy} $(\mathbf{x}, t)$, and $\sigma_{xy}(\mathbf{x}, t)$ are the stress components, ε_1 $(\mathbf{x}, t)$ is a field variable related to the dilatational wave, and $\varepsilon_2(\mathbf{x}, t)$ and $\varepsilon_3(\mathbf{x}, t)$ are field variables associated with the shear waves, p(x) denotes the density, and $\mathbf{f}(\mathbf{x}, t) = (f_x, f_y)$ are the body forces per unit volume. Quantity $\hat{\lambda} = (\lambda + \mu)M_{u1} - \mu M_{u2}$ and $\hat{\mu} = \mu M_{u2}$ are the high-frequency limit or unrelaxed Lame constants, with λ and μ as the low-frequency limit or relaxed Lame constants, and $M_{u\nu} = \tau_\varepsilon^{(\nu)}/\tau_\sigma^{(\nu)}$ where $\tau_\varepsilon^{(\nu)}$ and $\tau_\sigma^{(\nu)}$ are the material relaxation times. Element $\nu = 1$ corresponds to the dilatational mode, and $\nu = 2$ to the shear modes. Finally, $\phi_\nu = (1 - \tau_\varepsilon^{(\nu)}/\tau_\sigma^{(\nu)})/\tau_\sigma^{(\nu)}$. The anelastic constitutive equation implicit in this formulation is the standard linear solid rheology (Carcione 1992a).

Equation (1) is expressed in the space of the physical coordinates (x, y) where the interfaces have arbitrary shapes. The physical mesh is transformed to a square computational domain by using the following generalized coordinates:

$$\xi = \xi(x, y), \qquad \eta = \eta(x, y). \tag{4}$$

The spatial derivatives are computed first with respect to the generalized coordinates ξ and η by using the Chebychev pseudospectral method, and afterward, the derivatives with respect to the physical variables x and y are calculated by using the chain rule. For example, if u is any of the variables of vector v given in equation (2a), the spatial derivatives in the physical space can be calculated as

$$\frac{\partial u}{\partial x} = \frac{\partial \xi}{\partial x}\frac{\partial u}{\partial \xi} + \frac{\partial \eta}{\partial x}\frac{\partial u}{\partial \eta}, \qquad \frac{\partial u}{\partial y} = \frac{\partial \xi}{\partial y}\frac{\partial u}{\partial \xi} + \frac{\partial \eta}{\partial y}\frac{\partial u}{\partial \eta}. \tag{5}$$

The metrics and the Jacobian of the transformation are calculated from

$$\frac{\partial \xi}{\partial x} = J\frac{\partial y}{\partial \eta}, \qquad \frac{\partial \xi}{\partial y} = -J\frac{\partial x}{\partial \eta},$$

$$\frac{\partial \eta}{\partial x} = -J\frac{\partial y}{\partial \xi}, \qquad \frac{\partial \eta}{\partial y} = J\frac{\partial x}{\partial \xi}, \tag{6}$$

$$J = \left(\frac{\partial x}{\partial \xi}\frac{\partial y}{\partial \eta} - \frac{\partial x}{\partial \eta}\frac{\partial y}{\partial \xi}\right)^{-1},$$

whose derivatives are also computed with the Chebychev operator. It is important to note that the transformations

allowed require continuous (smooth) curves and a nonsingular Jacobian.

THE NUMERICAL METHOD

The computational domain is a square region $(\xi, \eta) \in [-1, 1] \times [-1, 1]$, where the grid distribution is defined by the Gauss-Lobatto points. The spatial derivatives in equations (5) and (6) are computed via a variant of the fast Fourier transform (FFT) for the cosine transform (Gottlieb and Orszag, 1977; Kosloff et al., 1990).

The stability condition and the accuracy of the time integration scheme depend on the minimum grid spacing of the mesh. The super fine grid of the Chebychev mesh at the boundaries implies time steps of the order $O(N^{-2})$ (N is the number of grid points),* making the modeling algorithm highly inefficient. This problem is solved by stretching the grid at the boundaries to allow time steps of order $O(N^{-1})$, thus reducing considerably the computer time (see Kosloff and Tal-Ezer, 1993). For instance, for Lamb's problem (Lamb, 1904), a nonsymmetric stretching function with denser grid at the surface than at the center is used in the vertical direction (Kosloff et al., 1990; Carcione, 1992a) to properly model the free surface boundary condition. In the horizontal direction, a symmetric stretching function is implemented (Kosloff and Tal-Ezer, 1993). For problems having more complex (curved) geometries, the stretchings are treated separately to take care of the minimum grid size explicitly.

The 2-D Chebychev operator is very sensitive to the boundary conditions. Each time the right hand side of (1) is computed, the boundary conditions are implemented. However, a direct application of these conditions produces instabilities (Gottlieb et al., 1982). This problem is solved by decomposing the wavefield into one-way modes (or characteristics) perpendicular to the boundaries and modifying these modes according to the boundary conditions. The method was recently applied by Thompson (1990) to fluid dynamic problems and by Kosloff et al. (1990) and Carcione (1992b) to the elastic and viscoelastic wave equations, respectively. The boundary treatment along a given direction requires the characteristic equation corresponding to equation (1) in that direction. Let us consider the boundary normal to the y-direction. Equation (1) can be expressed as

$$\frac{\partial \mathbf{v}}{\partial t} = \underset{\sim}{\mathbf{B}} \frac{\partial \mathbf{v}}{\partial y} + \mathbf{s}_y,$$

where

$$\mathbf{s}_y = \underset{\sim}{\mathbf{A}} \frac{\partial \mathbf{v}}{\partial x} + \mathbf{s}. \tag{7}$$

After local diagonalization of matrix $\underset{\sim}{\mathbf{B}}$ as $\underset{\sim}{\mathbf{B}} = \underset{\sim}{\mathbf{S}} \underset{\sim}{\Lambda} \underset{\sim}{\mathbf{S}}^{-1}$, equation (7) can be written as

$$\frac{\partial \mathbf{v}}{\partial t} = \underset{\sim}{\mathbf{S}} \mathcal{H} + \mathbf{s}_y, \tag{8}$$

*Near the boundary of the mesh, the smallest distance between two points is proportional to N^{-2}. This affects the stability of the time integration scheme which considers the minimum grid spacing.

the characteristic equation, where

$$\mathcal{H} \equiv \underset{\sim}{\Lambda} \underset{\sim}{\mathbf{S}}^{-1} \frac{\partial \mathbf{v}}{\partial y} \tag{9}$$

are the characteristic variables. $\underset{\sim}{\Lambda}$ is a diagonal matrix formed with the eigenvalues of $\underset{\sim}{\mathbf{B}}$, $\lambda_i = 1, \ldots, 8$ related to the phase velocities of the outgoing and incoming wave modes such that $\mathcal{H}$ represents each decoupled characteristic mode in the y-direction. Equation (8) completely defines $\partial \mathbf{v}/\partial t$ at the boundaries in terms of the decoupled outgoing and incoming modes. The characteristics $\mathcal{H}_i$, with $\lambda_i > 0$, represent traveling modes in the positive direction of the coordinate axes, and vice versa for those characteristics with $\lambda_i < 0$. Having this in mind, the incoming modes are those quantities that point in toward the computational domain. These characteristics are computed from the boundary conditions, while the outgoing modes are not modified, and replaced back into equation (8) to get the equations for the boundaries. The directions of the characteristics at the boundaries are illustrated in Figure 1. The boundary equations for the upper (upper sign) and lower (lower sign) boundaries of the numerical mesh are now given.

The Neumann boundary equations are

$$\dot{v}_x^{(new)} = \dot{v}_x^{(old)} + \frac{1}{Z_S} (\pm \dot{\sigma}_{xy}^{(old)} - \dot{f}), \tag{10a}$$

$$\dot{v}_y^{(new)} = \dot{v}_y^{(old)} \pm \frac{1}{Z_P} (\dot{\sigma}_{yy}^{(old)} - \dot{g}), \tag{10b}$$

$$\dot{\sigma}_{xx}^{(new)} = \dot{\sigma}_{xx}^{(old)} - \frac{\hat{\lambda}}{\hat{E}} (\dot{\sigma}_{yy}^{(old)} - \dot{g}), \tag{10c}$$

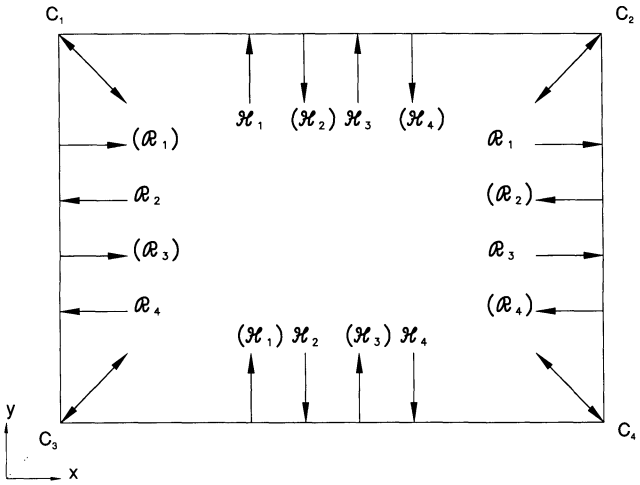

FIG. 1. Horizontal ($\mathcal{R}$) and vertical ($\mathcal{H}$) characteristics at the boundaries of the numerical mesh. The characteristics at the corners are also indicated. Subscripts 1 and 2 correspond to the 1-D compressional waves and subscripts 3 and 4 to the shear waves. Those quantities between parentheses (the incoming modes) are computed from the boundary conditions.

$$\dot{\sigma}_{yy}^{(new)} = \dot{g}, \tag{10d}$$

$$\dot{\sigma}_{xy}^{(new)} = \pm\dot{f}, \tag{10e}$$

$$\dot{\varepsilon}_1^{(new)} = \dot{\varepsilon}_1^{(old)} + \frac{\phi_1}{\hat{E}}\,(\dot{g} - \dot{\sigma}_{yy}^{(old)}), \tag{10f}$$

$$\dot{\varepsilon}_2^{(new)} = \dot{\varepsilon}_2^{(old)} - \frac{\phi_2}{\hat{E}}\,(\dot{g} - \dot{\sigma}_{yy}^{(old)}), \tag{10g}$$

$$\dot{\varepsilon}_3^{(new)} = \dot{\varepsilon}_3^{(old)} + \frac{\phi_2}{\hat{\mu}}\,(\pm\dot{f} - \dot{\sigma}_{xy}^{(old)}), \tag{10h}$$

where f and g are time-dependent functions, and $Z_P = (\hat{E}\rho)^{1/2}$ and $Z_S = (\hat{\mu}\,\rho)^{1/2}$ are the unrelaxed compressional and shear impedances of the medium. A dot above a variable denotes time differentiation. The superscript *(old)* indicates the variables given by equation (l), and the superscript (new) refers to the variables of the left-hand side of equation (8), after modification of the incoming characteristics. In practice, at every time step and after application of the differential operator, the vector of field variables is modified according to the boundary equations. Note that $f = g = 0$ gives free-surface boundary conditions. The method can also be used to introduce a source function at a given point of the boundary. For instance, $f = 0$ and $\dot{\sigma}_{yy}(\mathbf{x}_0, t) = \dot{g}(t)$ is a vertical force located at $\mathbf{x}_0$ with time history *g(t).*

The Dirichlet boundary equations are

$$\dot{v}_x^{(new)} = \dot{v}, \tag{11a}$$

$$\dot{v}_y^{(new)} = \pm\dot{w}, \tag{11b}$$

$$\dot{\sigma}_{xx}^{(new)} = \dot{\sigma}_{xx}^{(old)} + \frac{\lambda}{\hat{E}}\,(\dot{\sigma}_{yy}^{(new)} - \dot{\sigma}_{yy}^{(old)}), \tag{11c}$$

$$\dot{\sigma}_{yy}^{(new)} = \dot{\sigma}_{yy}^{(old)} + Z_P\,(\pm\dot{v}_y^{(old)} - \dot{w}), \tag{11d}$$

$$\dot{\sigma}_{xy}^{(new)} = \dot{\sigma}_{xy}^{(old)} \pm Z_S(\dot{v}_x^{(old)} - \dot{v}), \tag{11e}$$

$$\dot{\varepsilon}_1^{(new)} = \dot{\varepsilon}_1^{(old)} - \rho\,\frac{\phi_1}{Z_P}\,(\dot{w} \mp \dot{v}_y^{(old)}), \tag{11f}$$

$$\dot{\varepsilon}_2^{(new)} = \dot{\varepsilon}_2^{(old)} + \rho\,\frac{\phi_2}{Z_P}\,(\dot{w} \mp \dot{v}_y^{(old)}), \tag{11g}$$

$$\dot{\varepsilon}_3^{(new)} = \dot{\varepsilon}_3^{(old)} \mp \rho\,\frac{\phi_2}{Z_S}\,(\dot{u} - \dot{v}_x^{(old)}), \tag{11h}$$

where w and v are time dependent functions. For instance, rigid boundary conditions imply $w = v = 0$.

The nonreflecting boundary equations are

$$\dot{v}_x^{(new)} = \frac{1}{2}\left(\dot{v}_x^{(old)} \pm \frac{1}{Z_S}\,\dot{\sigma}_{xy}^{(old)}\right), \tag{12a}$$

$$\dot{v}_y^{(new)} = \frac{1}{2}\left(\dot{v}_y^{(old)} \pm \frac{1}{Z_P}\,\dot{\sigma}_{yy}^{(old)}\right), \tag{12b}$$

$$\dot{\sigma}_{xx}^{(new)} = \dot{\sigma}_{xx}^{(old)} - \frac{\lambda}{2\hat{E}}\,(\dot{\sigma}_{yy}^{(old)} \mp Z_P\dot{v}_y^{(old)}), \tag{12c}$$

$$\dot{\sigma}_{yy}^{(new)} = \frac{1}{2}\,(\dot{\sigma}_{yy}^{(old)} \pm Z_P\dot{v}_y^{(old)}), \tag{12d}$$

$$\dot{\sigma}_{xy}^{(new)} = \frac{1}{2}\,(\dot{\sigma}_{xy}^{(old)} \pm Z_S\dot{v}_x^{(old)}), \tag{12e}$$

$$\dot{\varepsilon}_1^{(new)} = \dot{\varepsilon}_1^{(old)} - \frac{\phi_1}{2\hat{E}}\,(\dot{\sigma}_{yy}^{(old)} \mp Z_P\dot{v}_y^{(old)}), \tag{12f}$$

$$\dot{\varepsilon}_2^{(new)} = \dot{\varepsilon}_2^{(old)} + \frac{\phi_2}{2\hat{E}}\,(\dot{\sigma}_{yy}^{(old)} \mp Z_P\dot{v}_y^{(old)}), \tag{12g}$$

$$\dot{\varepsilon}_3^{(new)} = \dot{\varepsilon}_3^{(old)} - \frac{\phi_2}{2\hat{\mu}}\,(\dot{\sigma}_{xy}^{(old)} \mp Z_S\dot{v}_x^{(old)}). \tag{12h}$$

The equations for the left boundary can be obtained from the upper boundary equations by substitutingx $\rightarrow$ y, y $\rightarrow x$, and $\varepsilon_2 \rightarrow -\varepsilon_2$. Similarly, the equations for the right boundary are obtained from the left boundary equations by substitutingx $\rightarrow -x$, where in this case, $v_x \rightarrow -v_x$, $\sigma_{xy} \rightarrow -\sigma_{xy}$, and $\varepsilon_3 \rightarrow -\varepsilon_3$.

When the boundary is not perpendicular to any of the Cartesian coordinate axes; i.e., when the y′-direction (system S') normal to the boundary does not coincide with the y-axis (system S) where the problem is solved, the boundary treatment is applied to the variables in system S', and then the boundary equations are obtained by the inverse rotation transformations. For the corner points, I use an "ad hoc" treatment introduced by Lie (1991, Forsvarets Forsknings Institut/Rapport-91/7009, Norwegian Defence Research Establishment), who defines the "normal to the corner point" inwards and bisecting the angle between the adjacent boundary lines (see Figure 1). For more details, see Carcione and Wang (1993).

EXAMPLES

The first example solves Lamb's problem to check the accuracy of the Chebychev operator. When the source is very close to the free surface, the high amplitude of the Rayleigh wave represents a challenge to the boundary treatment. The second example simulates wave propagation in a model formed by a mount at the surface and a synclinal structure in depth. The third example illustrates wave propagation through a surface step to test the 1-D transformations and the characteristic approach applied to the corner points. Finally, the last example computes snapshots in an anticlina1 structure containing a stack of fine layers.

Lamb's problem.– T h i s example simulates Lamb's problem with compressional and shear velocities of $c_P = (E/\rho)^{1/2} = 2000$ m/s, and $c_S = (\mu/\rho)^{1/2} = 1155$ m/s, respectively, a density of $\rho = 1$ g/cm^3, and with the choice $\tau_\varepsilon^{(\nu)} = \tau_\sigma^{(\nu)}$, $\nu = 1, 2$, giving the elastic wave equation in the low-frequency limit. The source is a vertical impact having a Ricker wavelet time-history with central frequency of $f_0 = 11$ Hz.

The calculations use a numerical mesh with $N_x = 121$ and $N_y = 81$ and with free surface boundary conditions applied to the upper boundary and open (nonreflecting) radiation conditions to the other boundaries. The size of the mesh is

designed to have 2.5 grid points per minimum shear wavelength at the center of the grid. Since for nonvertical incidence the incoming waves are not completely eliminated, absorbing strips are used at the sides and lower boundary to eliminate the residual nonphysical reflections (Kosloff and Kosloff, 1986). The solution is propagated to 2 s, with a time step of 1 ms by using a fourth-order Runge-Kutta integration scheme (Carcione, 1992a). Comparisons between numerical and analytical elastic solutions are shown in Figure 2 where the coordinates of the receivers relative to the source are (a) (720, 0) m and (b) (720, 290) m. As can be seen from the pictures, the results are satisfactory.

Mount and syncline model.– The numerical mesh of this second example, which uses the 1-D mapping functions of Lamb's problem, is illustrated in Figure 3. Also, the same source type and number of grid points as in the previous example are considered, but in this case the upper region above the syncline is anelastic with the relaxed (elastic) velocities of Lamb's problem. Anelasticity is modeled by one dissipation mechanism with bulk and shear quality factors of Q_k = 60 and Q_S = 40 at the central frequency of the source. The compressional and shear velocities of the lower region (see Figure 4) are c_P = 3000 m/s and c_S = 1500 m/s, respectively, with a density of ρ = 2 g/cm^3.

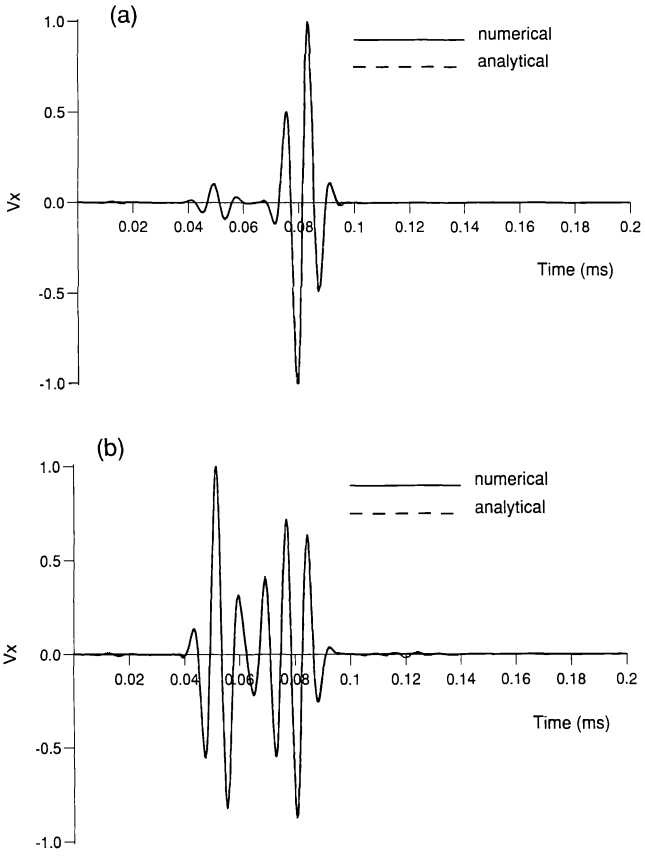

FIG. 2. Comparison between numerical and analytical solutions for Lamb's problem where the coordinates of the receivers with respect to the source are (a) (720,0) m and (b) (720, 290) m. The match is virtually perfect with a maximum error of less than one percent.

Figure 4 shows the elastic snapshots of the particle velocity vector at three successive propagation times. The amplitude of the surface wave is saturated to allow the propagation of the body waves to be easily visualized. The seismograms recorded near the surface are shown in Figure 5. The main signal is the Rayleigh wave, which shows attenuation and velocity dispersion.

Step model.– The model is a square mesh with two free surfaces at the upper and right edges, including a material interface at 525 m depth, separating two elastic media whose velocities and densities, as well as source type and number of grid points, are the same as in the previous example. The upper and right boundaries of the physical mesh satisfy traction-free conditions. The vertical mapping function of Lamb's problem is implemented in both spatial directions, taking a denser mesh at the step to correctly model the free surface boundary condition. The lower and left boundaries satisfy open radiation conditions. A vertical force is applied at grid point 90 located at 525 m from the corner and 1.86 m deep.

Figure 6 displays snapshots of the particle velocity vector at t = 0.6 s and t = 0.9 s. In the first picture, the compressional wave has been diffracted by the corner, while the Rayleigh wave is on the corner with the shear wave slightly in advance. At 0.9 s the Rayleigh wave has been split into transmitted and reflected surface waves traveling vertically and horizontally, respectively. Figure 7 represents the response of the medium recorded at 1.86 m from the surface. The first 60 receivers correspond to the upper boundary and the next 40 receivers to the right boundary of the step. The sequence of reflected and transmitted Rayleigh waves, from both the corner and the interface, can be seen.

Anticline of fine layers.– This example illustrates the ability of the method to model a stack of fine layers, one of the most common geological structures appearing in sedimentary formations. The grid geometry with $N_x = N_y = 8\ 1$ is shown in Figure 8, where the fine concentration of points at the center of the mesh has been obtained with the mapping

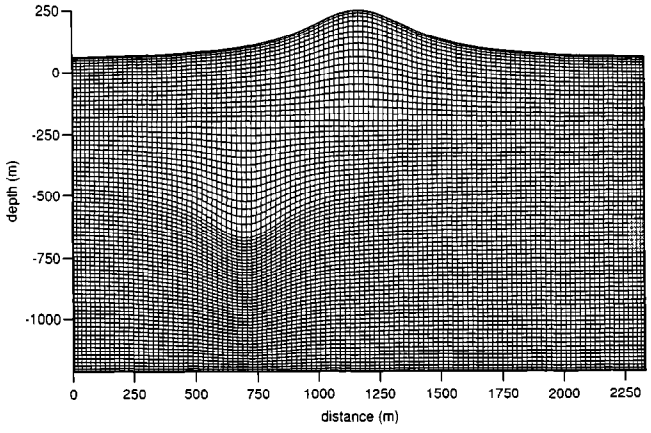

FIG. 3. Numerical mesh for the mount and syncline model. The upper boundary is a free surface and the others satisfy nonreflecting boundary conditions.

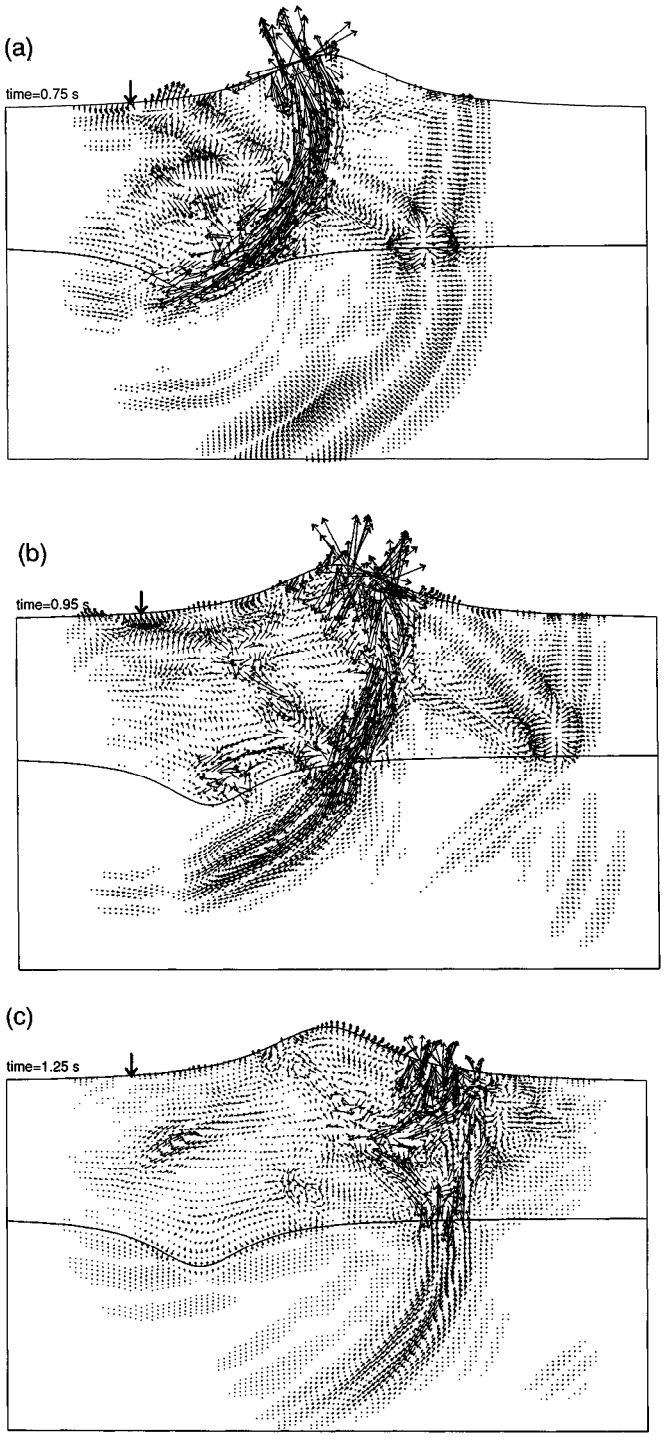

FIG. 4. Elastic snapshots of the particle velocity vector at (a) 0.75 s, (b) 0.95 s, and (c) 1.25 s. The amplitudes on the plot were gained to allow the propagating body waves to be easily visualized, leading to saturation of the large amplitude surface waves.

function introduced by Augenbaum (1990) (the upper boundary is a free surface). This shows that it is more effective to use mapping transformations to resolve the structure than to simply add more grid points into the physical coordinate system.

The anticline structure is a periodic set of sandstone-limestone layers (from grid point 35 to grid point 47) of equal thickness embedded in homogeneous sandstone. The spatial period of the stratification is approximately 4 m, such that the total thickness of the system is approximately 25 m. In Carcione et al. (1991) can be found the values of the wave velocities and elastic constants of the equivalent medium. The sandstone is viscoelastic with bulk and shear quality factors of $Q_k = 40$ and $Q_s = 20$ at the central frequency of the source. At the center of the anticline, a vertical force of central frequency 17.5 Hz excites the medium. The ratio of dominant wavelength to spatial period for vertical incidence is equal to 40 for the P-waves and to 22 for the S-waves, so the long-wavelength approximation is satisfied, and the medium behaves as an anisotropic medium (e.g., Carcione et al., 1991).

The solution is propagated to 1.2 s with a time step of 0.25 ms. Figure 9 shows snapshots of the particle velocity vector at three different propagation times. This example illustrates the performance of the differential operator in regions where sharp discontinuities of the material properties occur.

The 2-D mesh generator used in the examples is far from optimum. More flexible techniques can be found in the computational fluid dynamics literature; for instance, the methods described in Thompson et al. (1985). The technique implemented by Nielsen et al. (1992), based on a multi-block strategy where the whole mesh is divided into subgrids containing homogeneous material properties, is also promising.

CONCLUSIONS

The present method solves the equations of dynamic viscoelasticity in heterogeneous media with arbitrary shaped smooth boundaries. Neumann and/or Dirichlet boundary conditions can be imposed at the four boundaries of the mesh. In addition, spatial grid adaptation by appropriate 1-D mapping functions allows a more accurate modeling of complex structures, and reduction in the computational cost by increasing the minimum grid spacing. The technique has immediate application to domain decomposition since the subdomains can be joined by imposing the appropriate boundary conditions on the incoming waves at the interfaces. In this way, different geometrical features, rheologies, and algorithms can be implemented in the same model (Carcione, 1991). Furthermore, the mesh generator can be improved by using techniques already applied in other areas of research like for instance computational fluid dynamics.

ACKNOWLEDGMENTS

This work was supported in part by the Commission of the European Communities under the GEOSCIENCE project.

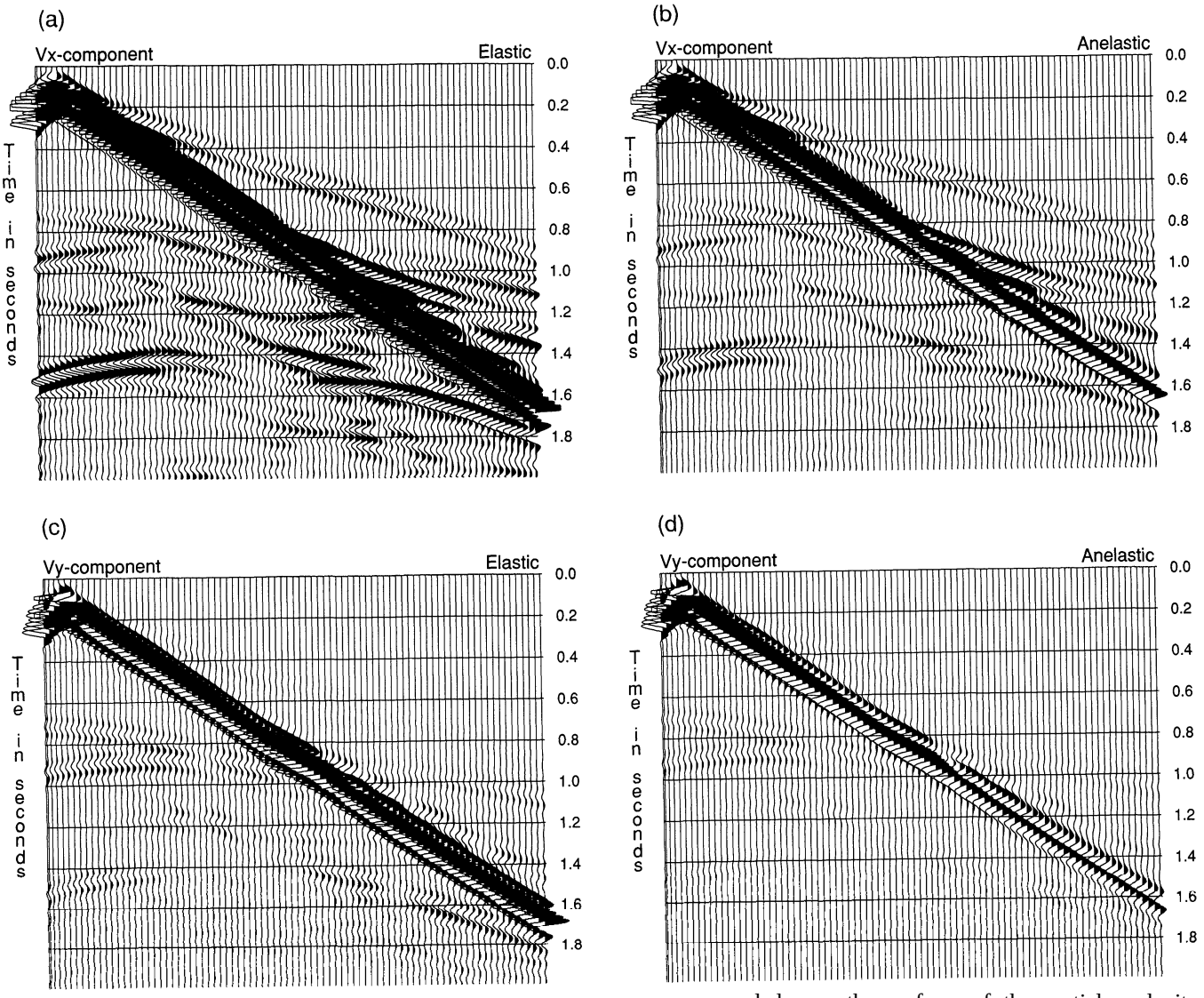

FIG 5 Elastic [(a) and (c)] and anelastic [(b) and (d)] seismograms, recorded near the surface, of the particle velocity components corresponding to the mount and syncline model. Attenuation and velocity dispersion of the Rayleigh wave can be observed.

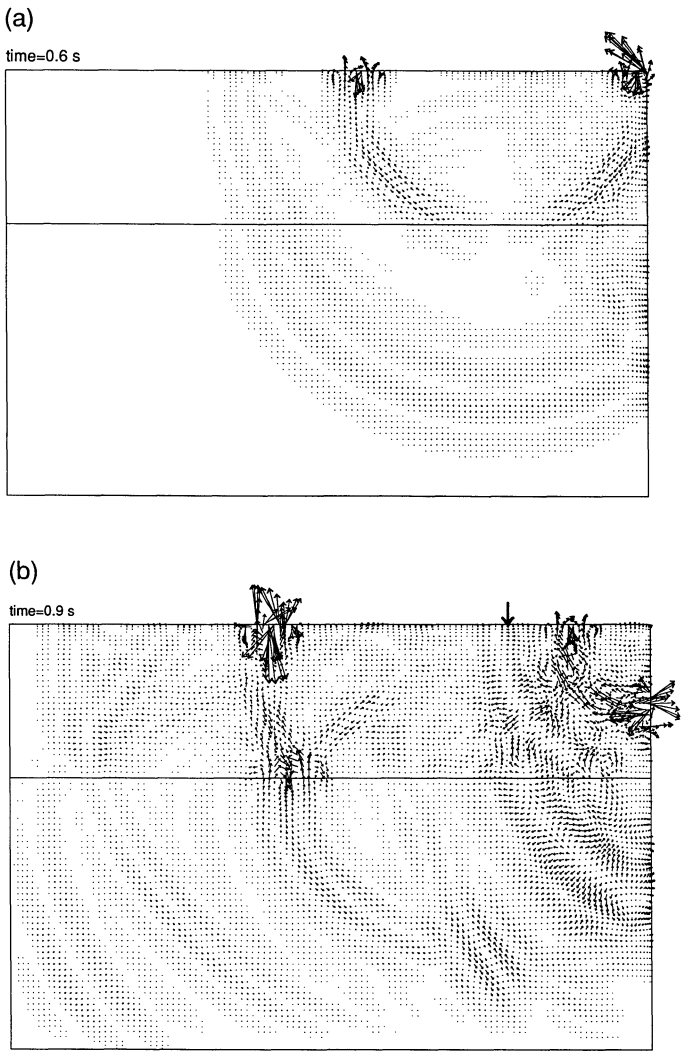

FIG. 6. Snapshots of the particle velocity vector for the step problem at (a) 0.6 s and (b) 0.9 s. In (a) the Rayleigh wave produced by a vertical impact has reached the corner. The reflected and transmitted surface waves can be observed in (b).

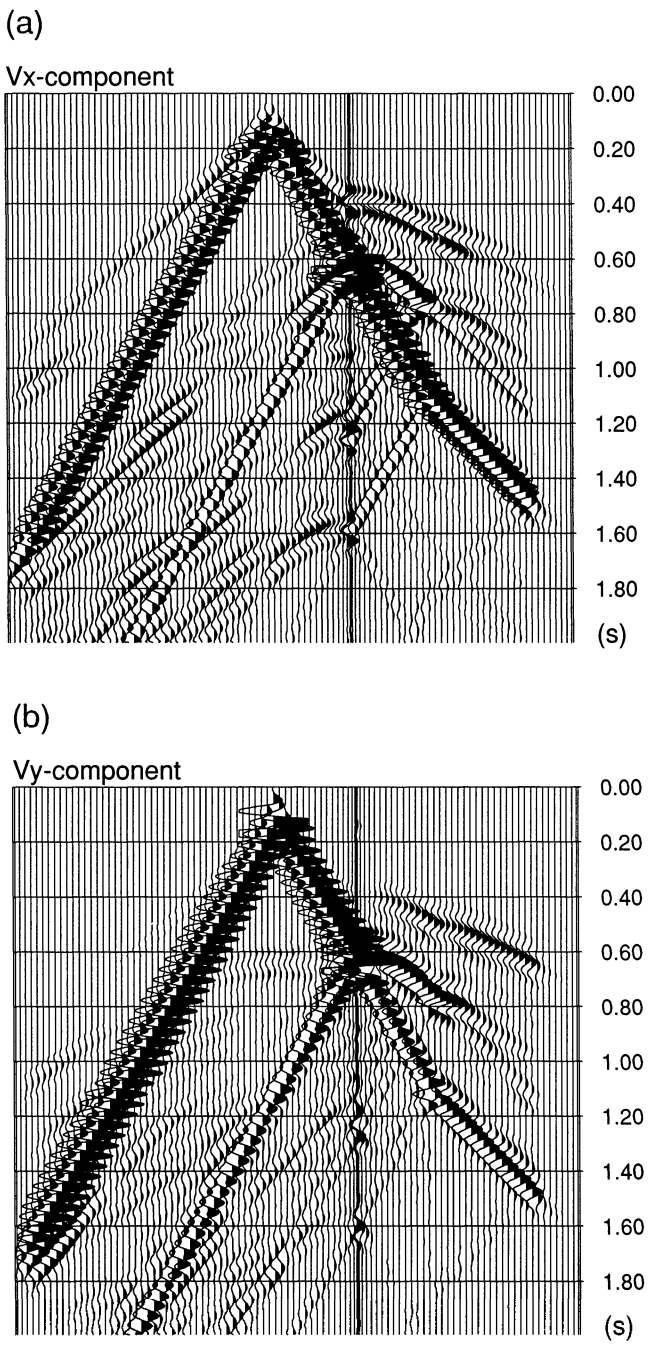

FIG. 7. Response of the step recorded at 1.86 m from the surface in (a) the horizontal component and (b) the vertical component. The first 60 receivers correspond to the upper boundary and the next 40 receivers to the right boundary of the step. The strong event is the Rayleigh wave that splits into transmitted and reflected Rayleigh waves at 0.6 s.

REFERENCES

Augenbaum, J. M., 1989, An adaptive pseudospectral method for discontinuous problems: Appl. Num. Math., 5, 459-480.

- 1990, Multidomain adaptive pseudospectral methods for acoustic wave propagation in discontinuous media: in Lee, D., Cakmak, A., and Vichnevetsky, R., Eds., Computational acoustic, seismo-ocean acoustics and modeling: North-Holland Publ. co., 19-40.

Carcione, J. M., 1991, Domain decomposition for wave propagation problems: J. Sci. Comput., 6, 453-472.

- 1992a, Modeling anelastic singular surface waves in the earth: Geophysics, 57, 781-792.

- 1992b, Boundary conditions for wave propagation problems: Presented at Internat. Conf. Spectral High Order Meth.

Carcione, J. M., Kosloff, D., and Behle, A., 1991, Long-wave anisotropy in stratified media: A numerical test: Geophysics, 56, 245-254.

Carcione, J. M., and Wang, J. P., 1993, A Chebyshev collocation method for the elastodynamic equation in generalized coordinates: Comput. Fluid Dynamics J., 2, 269-290.

Fornberg, B., 1988, The pseudospectral method: Accurate representation of interfaces in elastic wave calculations: Geophysics, 53, 625-637.

Gottlieb, D., Gunzburger, M., and Turkel, E., 1982, On numerical boundary treatment for hyperbolic systems: SIAM J. Numer. Anal., 13, 671-697.

Gottlieb, D., and Orszag, S., 1977, Numerical analysis of spectral methods: Theory and applications: Soc. Indust. and Appl. Math.

Kessler, D., and Kosloff, D., 1990, Acoustic wave propagation in 2-D cylindrical coordinates: Geophys . J. Internat., 103, 577-587.

Kosloff, D., Kessler, D., Queiroz Filho, A., Tessmer, E., Behle, A., and Strahilevitz, R., 1990, Solution of the equations of dynamic elasticity by a Chebychev spectral method: Geophysics, 55, 734-748.

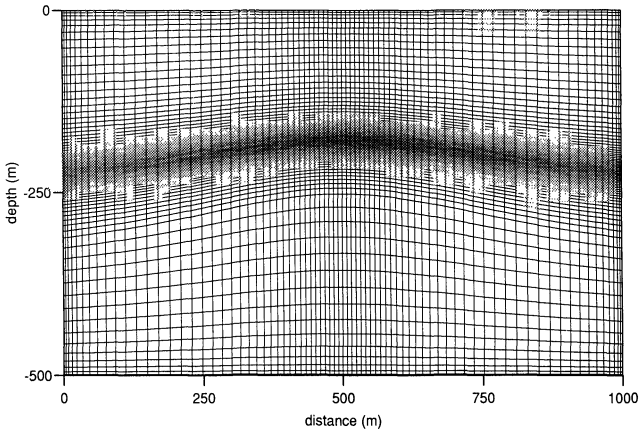

FIG. 8. Numerical mesh of the physical space for the fine layering problem. The region of the anticline has a vertical grid spacing of 2 m and represents a periodic sequence of sandstone (anelastic)-limestone (elastic) layers.

Kosloff, R., and Kosloff, D., 1986, Absorbing boundaries for wave propagation problems: J. Comput. Phys., 63, 363-376.
Kosloff, D., and Tal-Ezer, H., 1993, A modified Chebyshev pseudospectral method with an $O(N^{-1})$ time step restriction: J. Comp. Phys., 104, 457-469.
Lamb, H., 1904, On the propagation of tremors over the surface of an elastic solid: Phi. Trans. Roy. Soc. (London), A 203, 1-42.
Nielsen, P., Berg, P., If, F., and Skovgaard, O., 1992, Using the pseudospectral method on curved grids for seismic forward modeling: 54th Mtg. and Tech. Exhib., Europ. Assoc. Expl. Geophys., Expanded Abstracts, 150-151.
Orszag, S. A., 1980, Spectral methods for problems in complex geometries: J. Comput. Phys., 37, 70-92.
Raggio, G. A., 1986, Pseudo spectral Chebyshev scheme for-forward acoustic modeling: Z. Angew. Math. Mech., 66, 545-553.
Tessmer, E., Kessler, D., Kosloff, D., and Behle, A., 1992a, Multi-domain Chebyshev-Fourier method for the solution of the equation of motion of dynamic elasticity: J. Comput. Phys., 100, 355-363.
Tessmer, E., Kosloff, D., and Behle, A., 1992b, Elastic wave propagation in the presence of surface topography: Geophys. J. Internat., 108, 621-632.
Thompson, K. W., 1990, Time-dependent boundary conditions for hyperbolic systems, II: J. Comput. Phys., 89, 439461.
Thompson, J. F., Warsi, Z. U. A., Wayne Mastin, C., 1985, Numerical grid generation, foundations and applications, North-Holland Publ. Co.
Wang, J. P., Nakamura, Y., and Yasuhara, M., 1991, A Chebyshev collocation method for the compressible Navier-Stokes equations in generalized coordinates: Trans. Japan Soc. Aero. Space Sci.,, 33, 120-134.

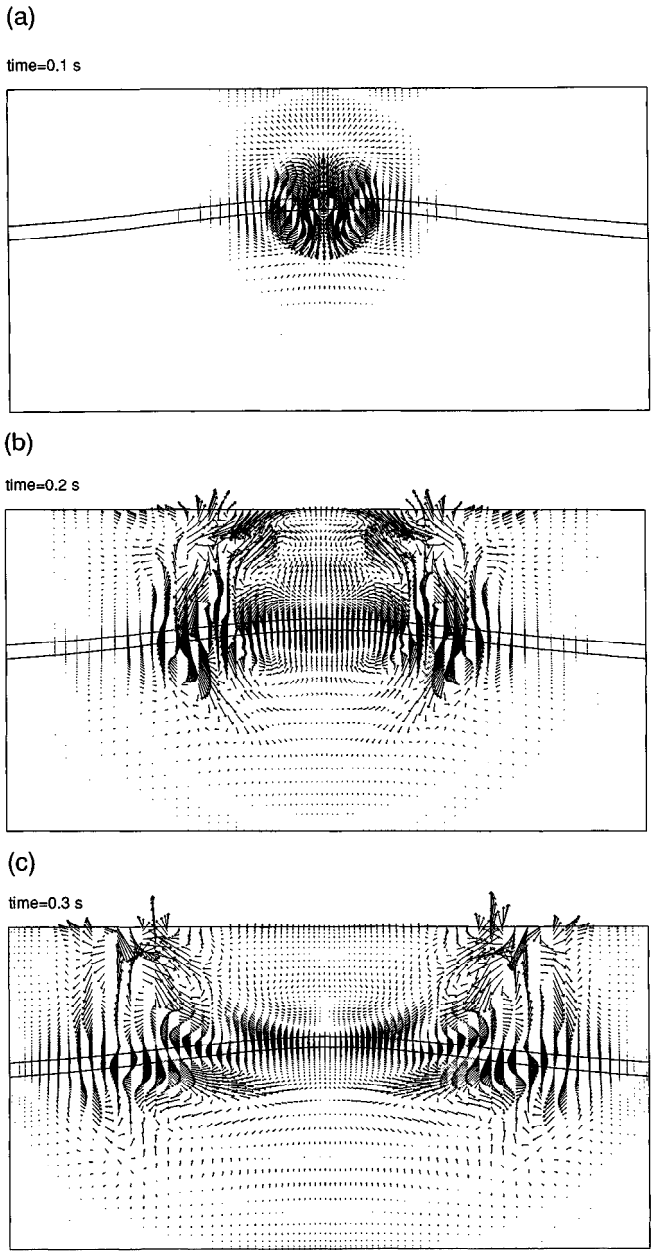

FIG. 9. Snapshots of the particle velocity vector at (a) 0.1 s, (b) 0.2 s, and (c) 0.3 s for the anticline model.